Active disturbance rejection attitude control of unmanned quadrotor via paired coevolution pigeon-inspired optimization

Yang Yuan and Haibin Duan
School of Automation Science and Electrical Engineering, Beihang University (BUAA), Beijing, China

Abstract

Purpose – The purpose of this paper is to develop a novel active disturbance rejection attitude controller for quadrotors and propose a controller parameters identification approach to obtain better control results.

Design/methodology/approach – Aiming at the problem that quadrotor is susceptible to disturbance in outdoor flight, the improved active disturbance rejection control (IADRC) is applied to design attitude controller. To overcome the difficulty that adjusting the parameters of IADRC controller manually is complex, paired coevolution pigeon-inspired optimization (PCPIO) algorithm is used to optimize the control parameters.

Findings – The IADRC, where nonlinear state error feedback control law is replaced by non-singular fast terminal sliding mode control law and a third-order tracking differentiator is designed for second derivative of the state, has higher control accuracy and better robustness than ADRC. The improved PIO algorithm based on evolutionary mechanism, named PCPIO, is proposed. The optimal parameters of ADRC controller are found by PCPIO with the optimization criterion of integral of time-weighted absolute value of the error. The effectiveness of the proposed method is verified by a series of simulation experiments.

Practical implications – IADRC can improve the accuracy of attitude control of quadrotor and resist external interference more effectively. The proposed PCPIO algorithm can be easily applied to practice and can help the design of the quadrotor control system.

Originality/value – An improved active disturbance rejection controller is designed for quadrotor attitude control, and a hybrid model of PIO and evolution mechanism is proposed for parameters identification of the controller.

Keywords Quadrotor, Pigeon-inspired optimization, Improved active disturbance rejection control, Non-singular fast terminal integral sliding mode, Population diversity, Evolutionary mechanism

Paper type Research paper

Introduction

In recent years, quadrotor has drawn a lot of attention with advantages of simple operation, low cost and high reliability (Wang *et al.*, 2020). As a kind of unmanned aerial vehicle (UAV), quadrotor has more competence when performing dull, dirty and dangerous task than manned aerial vehicle (Labbadi and Cherkaoui, 2019). For example, in the battlefield of COVID-19 epidemic prevention and control, quadrotor has become the vanguard of epidemic prevention and control in the patrol field and played an important role in the prevention of infection. In addition, quadrotor has been widely used in the field such as aerial photography, goods delivery and terrain exploration (Shao *et al.*, 2018).

Precise attitude control of quadrotor is fundamental and necessary to complete tasks, which has become an important research hotspot (Zhao *et al.*, 2019; Raza *et al.*, 2017), and it is a challenging task how to design a controller robust to external disturbance, noise, wind and actual parameter changes (Roohul *et al.*, 2016). A hybrid H2/H∞ static feedback tracking controller with measurement noise and external disturbance robustness is proposed, and the time response of mixed H2/H∞ controller is improved by increasing the regional pole assignment constraint (Emam and Fakharian, 2016). A control strategy combining feedback linearization and linear quadratic regulator is proposed to stabilize the attitude of the disturbed quadrotor (Zhao *et al.*, 2016). However, the linear control strategy cannot guarantee the tracking performance of quadrotor during active maneuverer (Tian *et al.*, 2019). To deal with the non-linearity and strong coupling of quadrotor system, sliding mode control has been introduced to UAV control (Ramirez-Rodriguez *et al.*, 2014). Nevertheless, ignoring external interference may result in poor robustness of the controller (Yang *et al.*, 2018a, 2018b). Observer-based flight control algorithm is designed to resist external disturbances. In addition to the design of the controller, an

The current issue and full text archive of this journal is available on Emerald Insight at: **https://www.emerald.com/insight/1748-8842.htm**

Aircraft Engineering and Aerospace Technology
94/2 (2022) 302–314
 [ISSN 1748-8842]
[DOI 10.1108/AEAT-07-2020-0136]

This work was partially supported by Science and Technology Innovation 2030-Key Project of "New Generation Artificial Intelligence" under Grant #2018AAA0102303, National Natural Science Foundation of China under Grant #U20B2071, #91948204, #U1913602 and #U19B2033.

Received 19 July 2020
Revised 7 April 2021
14 August 2021
Accepted 22 September 2021

observer is designed to approximate the disturbed state and external disturbance (Muhammad *et al.*, 2019; Rooh *et al.*, 2019). Furthermore, the control strategies such as adaptive or backstepping which are model-based are in stability risks in the presence of endogenous uncertainties and unknown input disturbances (Oliva-Palomo *et al.*, 2019).

Active disturbance rejection control (ADRC) is a nonlinear control strategy derived from proportion integration differentiation (PID) control, and it is independent of specific mathematical model of the controlled object and has strong robustness and anti-disturbance competence (Han, 2009). Due to these advantages, ADRC has attracted significant attentions from different engineering fields. ADRC is applied for electric power steering system with assist motor variable mode to reduce the disturbance caused by road surface (Ma *et al.*, 2018). To improve the robustness of the optimal control strategy of the finite control set, a sliding mode extended state observer is proposed to estimate the disturbance of the output effect (Wu and Li, 2018). In this paper, improved ADRC (IADRC) is developed. A novel non-singular fast terminal sliding mode (NFTSMC) control law is proposed to replace nonlinear state error feedback (NLSEF) control law, by which the tracking error converges in finite time and the control effect is improved. To obtain the second derivative of the state required by NFTSMC, a third-order tracking differentiator (TOTD) is designed. However, there are more parameters to be adjusted in IADRC compared with PID, and the trial and error tuning method is time-consuming and inefficient (Hai *et al.*, 2019). Hence, it is necessary that an efficient method to find the optimal parameters of the controller.

Pigeon-inspired optimization (PIO) is a bionic heuristic optimization algorithm which is based on the navigation behaviour of pigeons while homing (Duan and Qiao, 2014). Owing to the advantages of fast convergence and high search efficiency, PIO has been widely used in optimization problems (Deng and Duan, 2016; Alazzam *et al.*, 2020; Duan *et al.*, 2019). However, in the case of fewer pigeon numbers and less iteration, fast convergence rate would significantly reduce the diversity of the population, resulting in PIO may fall into local extremum (Duan and Wang, 2016; Zhang and Duan, 2017). Genetic algorithm (GA) is another well-known optimization algorithm that simulates the natural evolution process, which can maintain a rich population diversity by mutation operator and crossover operator (Srinivas and Patnaik, 1994). In this paper, the evolutionary mechanism of GA was introduced into PIO to improve the disadvantage of early maturity and increase population diversity. It is worth noting that in this paper, crossover and mutation operators are carried out for pairs of pigeons and will not be carried out with other individuals after pairs are determined. Then improved PIO, named paired coevolution pigeon-inspired optimization (PCPIO), is applied to optimize control parameters of IADRC to ensure control effect.

The contributions of this article are presented as follows. IADRC is developed for quadrotor attitude control, where a novel NFTSMC is developed to improve the accuracy and robustness of ADRC, and a TOTD is designed to provide input reference instead of original tracking differentiator. A PIO variant PCPIO is proposed to improve the problem of local convergence caused by fast decrease of population diversity in original PIO algorithm by introducing a diversity factor and coevolution mechanism. Compared with traditional ADRC and PID, the anti-disturbance ability of IADRC controller is verified. And the advantages of PCPIO is approved by the results of optimizing control parameters of IADRC controller in contrast to GA, PIO and particle swarm optimization (PSO) (Kennedy and Eberhart, 1995).

The remainder of this article is organized as follows. Section 2 presents the attitude dynamics of a quadrotor. Section 3 describes the design of IADRC attitude controller. Original PIO and its improved variant PCPIO are shown in Section 4. Section 5 presents stability and convergence analysis of proposed IADRC and PCPIO. Comparative simulation experiments and analysis are given in Section 6. Section 7 concludes the article.

Attitude dynamics of quadrotors

Quadrotor UAV has four individual electrical motors and six degrees of freedom including position motions and attitude motions, and the position and angle can be adjusted by changing the speed of the motors. The structure diagram of X-shaped quadrotor is shown in Figure 1. There are two reference frames subjected to the quadrotor: an earth-fixed frame $E = (O_E: X_E Y_E Z_E)$ and a body-fixed frame $B = (O_B: X_B Y_B Z_B)$ whose origin is located at the center of mass of the rigid body.

Figure 1 Quadrotor schematic

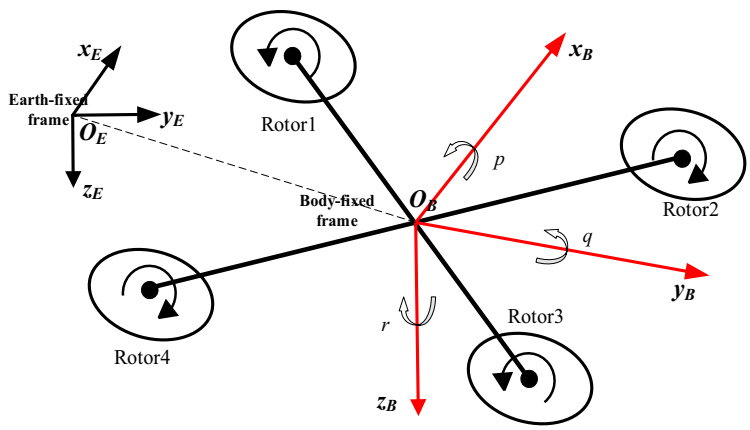

In this paper, the rotational dynamics model of the quadrotor is considered as (Quan, 2007):

$$\dot{\Theta}=W\Omega \tag{1}$$

$$\mathcal{J}\dot{\Omega}=-\Omega\times\mathcal{J}\Omega+\tau+G_a+\Delta \tag{2}$$

where $\Theta=(\phi,\theta,\psi)^{\mathrm{T}}\in\mathbb{R}^3$ is Euler angle, $\Omega=(p,q,r)^{\mathrm{T}}\in\mathbb{R}^3$ represents angular velocity, $\mathcal{J}\in\mathbb{R}^{3\times3}$ is the inertia matrix in the body-fixed frame, $\tau=(\tau_x,\tau_y,\tau_z)^{\mathrm{T}}\in\mathbb{R}^3$is control input torque, $G_a=(G_{a\phi},G_{a\theta},G_{a\psi})^{\mathrm{T}}\in\mathbb{R}^3$is gyroscopic moment, and $\Delta\in\mathbb{R}^3$ indicates disturbance and uncertainties. The matrix Wcan be calculated as:

$$W=\begin{bmatrix}1 & \sin\phi\tan\theta & \cos\phi\tan\theta\\ 0 & \cos\phi & -\sin\phi\\ 0 & \sin\phi/\cos\theta & \cos\phi/\cos\theta\end{bmatrix} \tag{3}$$

Assuming the speed of motor k is $(-1)^k\varpi^k(k=1,2,3,4)$, then the expression of G_a can be described as follows:

$$\begin{cases}G_a=\begin{bmatrix}\mathcal{J}_r q\Omega_r & -\mathcal{J}_r p\Omega_r & 0\end{bmatrix}^T\\ \Omega_r=\sum_{i=1}^{4}(-1)^{k+1}\varpi_k\end{cases} \tag{4}$$

where $\mathcal{J}_r$ represents total moment of inertia of motor rotor and propeller. τ is generated by rotors and can be given by:

$$\begin{bmatrix}T\\ \tau_x\\ \tau_y\\ \tau_z\end{bmatrix}=\begin{bmatrix}c_T & c_T & c_T & c_T\\ \frac{\sqrt{2}}{2}dc_T & -\frac{\sqrt{2}}{2}dc_T & -\frac{\sqrt{2}}{2}dc_T & \frac{\sqrt{2}}{2}dc_T\\ \frac{\sqrt{2}}{2}dc_T & \frac{\sqrt{2}}{2}dc_T & -\frac{\sqrt{2}}{2}dc_T & -\frac{\sqrt{2}}{2}dc_T\\ c_M & -c_M & c_M & -c_M\end{bmatrix}\begin{bmatrix}\varpi_1^2\\ \varpi_2^2\\ \varpi_3^2\\ \varpi_4^2\end{bmatrix} \tag{5}$$

where T is total force generated by all propellers, c_T is propeller pull factor, d is the distance of rotors from quadrotor mass center, and c_M is propeller moment coefficient.

According to the equations (1)–(4), the dynamic model of the quadrotor can be described as:

$$\begin{cases}\dot{p}=\frac{(\mathcal{J}_y-\mathcal{J}_z)qr}{\mathcal{J}_x}+\frac{\tau_x}{\mathcal{J}_x}+\frac{\mathcal{J}_r}{\mathcal{J}_x}q\Omega_r+\frac{\Delta_x}{\mathcal{J}_x}\\ \dot{q}=\frac{(\mathcal{J}_z-\mathcal{J}_x)pr}{\mathcal{J}_y}+\frac{\tau_y}{\mathcal{J}_y}-\frac{\mathcal{J}_r}{\mathcal{J}_y}p\Omega_r+\frac{\Delta_y}{\mathcal{J}_y}\\ \dot{r}=\frac{(\mathcal{J}_x-\mathcal{J}_y)pq}{\mathcal{J}_z}+\frac{\tau_z}{\mathcal{J}_z}+\frac{\Delta_z}{\mathcal{J}_z}\\ \dot{\phi}=p+(q\sin\phi+r\cos\phi)\tan\theta\\ \dot{\theta}=q\cos\phi-r\sin\phi\\ \dot{\psi}=\frac{1}{\cos\theta}(q\sin\phi+r\cos\phi)\end{cases} \tag{6}$$

Improved active disturbance rejection attitude control for quadrotors

By equation (6), attitude dynamic model can be described by (Yang *et al.*, 2018a, 2018b):

$$\begin{cases}\ddot{\phi}=\ddot{\psi}\sin(\theta)+\dot{\psi}\dot{\theta}\cos(\theta)+\left((\mathcal{J}_y-\mathcal{J}_z)qr+\mathcal{J}_r q\Omega_r+\Delta_x\right)/\mathcal{J}_x+\tau_x/\mathcal{J}_x\\ \ddot{\theta}=\dot{\theta}\dot{\phi}\tan(\phi)-\ddot{\psi}\tan(\phi)\cos(\theta)-\dot{\psi}\dot{\phi}\cos(\theta)+\dot{\psi}\dot{\theta}\tan(\phi)\sin(\theta)+\left((\mathcal{J}_z-\mathcal{J}_x)pr+\mathcal{J}_r p\Omega_r+\Delta_y\right)/\left(\mathcal{J}_y\cos(\phi)\right)+\tau_y/\left(\mathcal{J}_y\cos(\phi)\right)\\ \ddot{\psi}=\ddot{\theta}\tan(\phi)/\cos(\theta)+\dot{\theta}\dot{\phi}/\cos(\theta)+\dot{\psi}\dot{\theta}\tan(\theta)+\dot{\psi}\dot{\phi}\tan(\phi)+\left((\mathcal{J}_x-\mathcal{J}_y)pq+\Delta_z\right)/\left(\mathcal{J}_z\cos(\phi)\cos(\theta)\right)+\tau_z/\left(\mathcal{J}_z\cos(\phi)\cos(\theta)\right)\end{cases} \tag{7}$$

To simplify the analysis of the design of attitude IADRC controller, arrange equations (7) to adjust the form of IADRC controller:

$$\begin{cases}\dot{x}_1=x_2\\ \dot{x}_2=f(t)+bu\end{cases} \tag{8}$$

where b is constant value, u represents control input, $f(t)$ indicates nonlinear dynamics model and disturbance.

Then, the following can be obtained:

$$\begin{cases}f_\phi(t)=\ddot{\psi}\sin(\theta)+\dot{\psi}\dot{\theta}\cos(\theta)+\left((\mathcal{J}_y-\mathcal{J}_z)qr+\mathcal{J}_r q\Omega_r+\Delta_x\right)/\mathcal{J}_x\\ b_\phi u_\phi=\tau_x/\mathcal{J}_x\\ f_\theta(t)=\dot{\theta}\dot{\phi}\tan(\phi)-\ddot{\psi}\tan(\phi)\cos(\theta)-\dot{\psi}\dot{\phi}\cos(\theta)+\dot{\psi}\dot{\theta}\tan(\phi)\sin(\theta)+\left((\mathcal{J}_z-\mathcal{J}_x)pr+\mathcal{J}_r p\Omega_r+\Delta_y\right)/\left(\mathcal{J}_y\cos(\phi)\right)\\ b_\theta u_\theta=\tau_y/\left(\mathcal{J}_y\cos(\phi)\right)\\ f_\psi(t)=\ddot{\theta}\tan(\phi)/\cos(\theta)+\dot{\theta}\dot{\phi}/\cos(\theta)+\dot{\psi}\dot{\theta}\tan(\theta)+\dot{\psi}\dot{\phi}\tan(\phi)+\left((\mathcal{J}_x-\mathcal{J}_y)pq+\Delta_z\right)/\left(\mathcal{J}_z\cos(\phi)\cos(\theta)\right)\\ b_\psi u_\psi=\tau_z/\left(\mathcal{J}_z\cos(\phi)\cos(\theta)\right)\end{cases} \tag{9}$$

where $b_\phi = 1/\mathcal{J}_x$, $b_\theta = 1/\mathcal{J}_y$, $b_\psi = 1/\mathcal{J}_z$.

Basic ADRC controller comprises tracking differentiator (TD), extended state observer (ESO), and nonlinear state error feedback (NLSEF) control law (Han, 2009), while IADRC consists of TOTD, ESO and NFTSMC control law. PCPIO receives the output of IADRC controller and optimizes the control parameters of IADRC.

The output variable v_1 of TOTD is used to track the input signal v, and the output variable v_2 and v_3 are the first derivative and second derivative of v_1, respectively (Yang and Lu, 2006). The TOTD model can be written as (Figure 2):

$$\begin{cases} e_v = v_1 - v \\ \dot{v}_1 = v_2 \\ \dot{v}_2 = v_3 \\ \dot{v}_3 = -a_1 R^3 e_v - a_2 R^2 v_2 - a_3 R v_3 \end{cases} \tag{10}$$

where e_v is tracking error, a_1,a_2,a_3 and R are positive constants, and $a_2 \times a_3 > a_1$.

ESO is used to estimate and compensate the disturbance and uncertainties. The mathematical model of the second order ESO is presented as:

$$\begin{cases} e = z_1 - y \\ f_e = fal(e, \alpha_1, \delta) \\ f_{e1} = fal(e, \alpha_2, \delta) \\ \dot{z}_1 = z_2 - \beta_1 e \\ \dot{z}_2 = z_3 - \beta_2 f_e + b_0 u \\ \dot{z}_3 = -\beta_3 f_{e1} \end{cases} \tag{11}$$

where z_1 and z_2 are the estimate values of state x_1 and its differential, respectively, z_3 indicates external disturbance and uncertainty of the system, y denotes roll angle generated by quadrotor model, β_1, β_2 and β_0 are different gains of ESO, $[\beta_1, \beta_2, \beta_3] = [3\omega_0, 3\omega_0^2, \omega_0^3]$, ω_0 is a positive number, and $fal(\bullet)$ is a nonlinear function. The expression of $fal(\bullet)$ is given by:

$$fal(e, \alpha, \delta) = \begin{cases} \dfrac{e}{\delta^{1-\alpha}} & |e| \leqslant \delta \\ |e|^\alpha \cdot \mathrm{sign}(e) & |e| > \delta \end{cases} \tag{12}$$

where δ denotes the linear width of $fal(\bullet)$ function and α influences the degree of nonlinearity of the observer.

The non-singular fast terminal sliding mode surface is selected as:

$$s = e_1 + \lambda_1 sig^{\gamma_1}(e_1) + \lambda_2 sig^{\gamma_2}(e_2) \tag{13}$$

where $e_1 = v_1 - z_1$ and $e_2 = v_2 - z_2$, λ_1 and λ_2 are constants bigger than zero, γ_1 and γ_2 are constants and $1 < \gamma_2 < 2$. Pick the differential of s as:

$$\begin{aligned} \dot{s} &= e_2 + \lambda_1 \gamma_1 |e_1|^{\gamma_1 - 1} e_2 + \lambda_2 \gamma_2 |e_2|^{\gamma_2 - 1} \dot{e}_2 \\ &= e_2 + \lambda_1 \gamma_1 |e_1|^{\gamma_1 - 1} e_2 + \lambda_2 \gamma_2 |e_2|^{\gamma_2 - 1} (v_3 - f - b_0 u) \end{aligned} \tag{14}$$

Set $\dot{s}$ equal to zero and substitute observed value z_3 for f, then equivalent control component u_{eq} can be described as:

$$\begin{aligned} u_{eq} = \left(\lambda_2 \gamma_2 b_0 |e_2|^{\gamma_2 - 1}\right)^{-1} \big[& e_2 + \lambda_1 \gamma_1 |e_1|^{\gamma_1 - 1} e_2 \\ & + \lambda_2 \gamma_2 |e_2|^{\gamma_2 - 1} (v_3 - z_3) \big] \end{aligned} \tag{15}$$

The component to reach the surface s is designed as:

$$u_{re} = b_0^{-1} (k_1 s + k_2 sig^\rho(s)) \tag{16}$$

where $k_1 > 0$, $k_2 > 0$, and $0 < \rho < 1$. The final control input u is the sum of u_{eq} and u_{re}, where equivalent control component is responsible for steering the attitude states, and reach the surface component is applied to bring the attitude states to approach the neighborhood of sliding surface in finite time.

To apply the improved PIO to the design of IADRC, an appropriate objective function should be established. Parameters including a_0 and R in TOTD, β_{01}, β_{02}, β_{03}, α_{01}, α_{02} and δ in ESO, λ_1,λ_2,γ_1,γ_2,k_1,k_2, and ρ in NFTSMC control law which determine IADRC performance should be optimized. The control target of quadrotor is to make attitude to track the signal as quickly and accurately as possible, so integral of time-weighted absolute value of the error (Yang *et al.*, 2018a, 2018b) is selected as evaluation index, which can be described as:

$$\mathcal{J} = \int_0^\infty t|e(t)|dt \tag{17}$$

where t is system running time, e is error between reference angle signal and tracking angle signal.

Paired coevolution pigeon-inspired optimization

PIO is proposed by Duan *et al.* according to the research on the navigation strategies of pigeons in different stages of flight

Figure 2 Structure of IADRC controller optimized by PCPIO

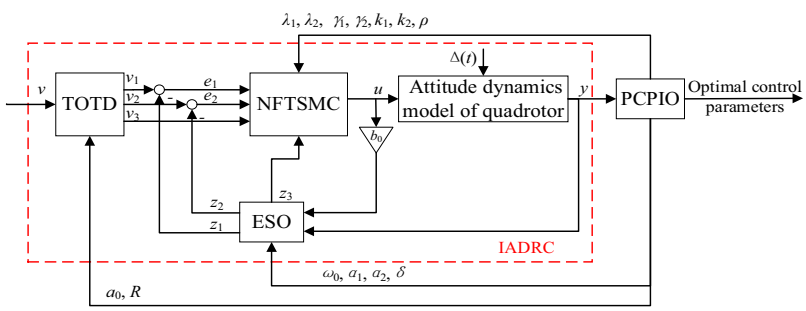

(Duan and Qiao, 2014). PIO is comprised by two operators. One is map and compass operator, which simulates the behavior of pigeons that treat the sun and earth magnetic fields as a navigation tool. Initialize N_p pigeons, and the i_{th} Pigeon has position $X_i = (X_{i1}, X_{i2},\ldots, X_{iD})$ and velocity $V_i = (V_{i1}, V_{i2},\ldots, V_{iD})$. Then, the pigeons will update in the D-dimensional search space in iteration n by map and compass operator first, which can be described as:

$$V_i(n) = V_i(n-1)\cdot e^{-Rn} + rand\cdot\left(X_{gbest} - X_i(n-1)\right) \tag{18}$$

$$X_i(n) = X_i(n-1) + V_i(n) \tag{19}$$

where R is map and compass factor, *rand* indicates a random number between 0 and 1, X_{gbest} is global optimal position. When n exceeds the map and compass iteration threshold N_{c1max}, Landmark operator begins to work, which simulates the impact of landmark navigation near destination on pigeons. Pigeons with poor knowledge of landmark would be abandoned, so the flock decreased by half at each iteration, which can be written as:

$$N_p(n) = \text{ceil}\left(\frac{N_p(n-1)}{2}\right) \tag{20}$$

Set the center of rest pigeons X_{center} as landmark, and the position of pigeons would be updated by:

$$X_i(n) = X_i(n-1) + rand\cdot\left(X_{center}(n) - X_i(n-1)\right) \tag{21}$$

$$X_{center}(n) = \frac{\sum_{i=1}^{N_p(n)} X_i(n)\cdot fitness(X_i(n))}{N_p\cdot\sum_{i=1}^{N_p(n)} fitness(X_i(n))} \tag{22}$$

where *fitness*() is a fitness function and can be defined as:

$$fitness(X_i) = \begin{cases} f_{\max}(X_i) \\ \dfrac{1}{f_{\min}(X_i)+\varepsilon} \end{cases} \begin{cases} \text{for maximization optimization problem} \\ \text{for minimization optimization problem} \end{cases} \tag{23}$$

During the exploration of map and compass operator, due to the leadership role of X_{gbest}, which adopts the experience of whole flock, the algorithm will perform poorly when X_{gbest} gets into local optimality and be difficult to escape.

In the map and compass operator of PIO algorithm, all particles move toward the global optimal position so that the diversity decreases rapidly after each iteration (Bartoszewicz and Nowacka-Leverton, 2010). If X_{gbest} falls into local extreme, other particles are difficult to escape from the extreme to find global optimal position. To keep the ability of exploration, the paper introduces mutation and crossover strategy of GA to map and compass operator to improve the diversity of PIO and increase the ability to jump out of local extreme. There is some modification on evolution mechanism, and the flow chart of PCPIO is shown in Figure 3.

First, the lower the diversity, the greater the probability of triggering GA. If diversity is greater than *rand*, then the mutation and crossover operators would be performed without other probability comparisons

Due to complex parameters of controller, there are differences among the upper and lower bounds of these parameters. To eliminate the impact caused by value range, normalization of X_{ij} is defined as:

Figure 3 Flow diagram of PCPIO for parameters identification of IADRC

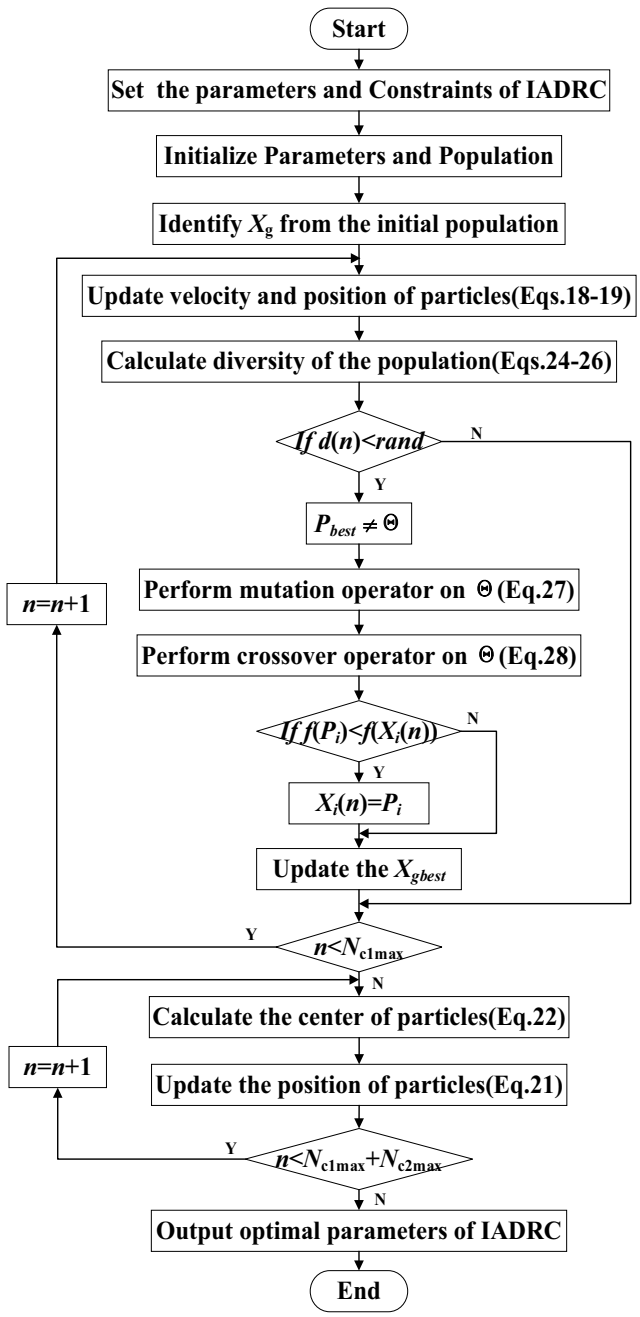

$$\tilde{X}_{ij}(n)=\frac{X_{ij}(n)-X_{j\min}}{X_{j\max}-X_{j\min}} \tag{24}$$

Then the diversity of the population can be measured as follows:

$$d(n)=\frac{\sum_{i=1}^{N_p}\sqrt{\sum_{j=1}^{D}\left(\tilde{X}_{ij}(n)-\overline{X}_j(n)\right)^2}}{N_p} \tag{25}$$

$$\overline{X}_j(n)=\frac{\sum_{i=1}^{N_p}\tilde{X}_{ij}(n)}{N_p} \tag{26}$$

where $d(n)$ is diversity of population in iteration n, and $\overline{X}_j(n)$ is the mean of population in j_{th} dimension.

Secondly, the set of person best swarm P_{best} is defined as Θ in each iteration, and the mutation operator is modified as:

$$P_{ij}(n)=\begin{cases}P_{ij}(n)+\left(X_{j\max}-P_{ij}(n)\right)\cdot r_1\cdot(1-n/N_{c\max}) & if\ rand0.5\\ P_{ij}(n)-\left(X_{ij}(n)-P_{j\min}\right)\cdot r_2\cdot(1-n/N_{c\max}) & if\ rand<0.5\end{cases} \tag{27}$$

where P_{ij} is j_{th} dimension of the individual optimality of the particle number i, r_1 and r_2 are two random numbers. The adaptive coefficient (1-$n/N_{c\max}$) of the operator results in that the mutation amplitude has a lager range at the exploration and a small range at the exploitation.

Third, to ensure that the i_{th} person best is still compared with the i_{th} current individual after each iteration, crossover operator is performed on i_{th} person best and $i+1_{th}$ person best as follows:

$$\begin{cases}P_i(n)=c\cdot P_i(n)+(1-c)\cdot P_{i+1}(n)\\ P_{i+1}(n)=c\cdot P_{i+1}(n)+(1-c)\cdot P_i(n)\end{cases} \tag{28}$$

where i = 1:2:popsize-1.

Finally, compare the fitness of P_i and X_i and the individual with small fitness become X_i.

Stability and convergence analysis

This chapter includes the stability analysis of IADRC and the convergence analysis of PCPIO.

Section A: stability analysis of improved active disturbance rejection control

The convergence of TOTD is firstly analyzed for IADRC. Rewrite equation (11) by Laplace transform as

$$\begin{cases}sV_1(s)-v_1(0)=V_2(s)\\ sV_2(s)-v_2(0)=V_3(s)\\ sV_3(s)-v_3(0)=-a_1R^3V_1(s)-a_2R^2V_2(s)-a_3RV_3(s)+a_1R^3V(s)\end{cases} \tag{29}$$

Above equation can be written in terms as:

$$\begin{aligned}&\left(a_1R^3+a_2R^2s+a_3Rs^2+s^3\right)V_1(s)\\&=s^2v_1(0)+sv_2(0)+v_3(0)+a_2R^2v_1(0)+a_3Rsv_1(0)\\&\quad+a_3Rv_2(0)+a_1R^3V(s)\end{aligned} \tag{30}$$

Divide both sides of the equation by a_1R^3, then $\lim_{R\to+\infty}\frac{V_1(s)}{V(s)}=1$, i.e. $\lim_{R\to+\infty}v_1=v$. Since a_1,a_2, a_3, $_R$ are positive, and $a_2\times a_3>a_1$, the system is asymptotically stable by Hurwitz stability criterion.

As for NFTSMC control law, choose Lyapunov function as $V=\frac{1}{2}s^2$, and its time derivative is:

$$\begin{aligned}\dot{V}&=s\left(e_2+\lambda_1\gamma_1|e_1|^{\gamma_1-1}e_2+\lambda_2\gamma_2|e_2|^{\gamma_2-1}(v_3-f-b_0u)\right)\\&=s\left(\lambda_2\gamma_2|e_2|^{\gamma_2-1}(z_3-f-b_0u_{re})\right)\\&=-s^T\lambda_2\gamma_2|e_2|^{\gamma_2-1}\left(k_1s+k_2sig^\rho(s)-(f-z_3)\right)\end{aligned} \tag{31}$$

Many researches have been conducted on the convergence of ESO (Guo and Zhao, 2011; Zhao and Guo, 2015). In this paper, it is assumed that absolute value of $f-z_3$ is bounded a positive constant d. Then we can continue to derive the formula as follow

$$\begin{aligned}\dot{V}&\le-s^T\lambda_2\gamma_2|e_2|^{\gamma_2-1}(k_1s+k_2sig^\rho(s)-d)\\&\le\Xi\left(-s^Tk_1s-s^Tk_2sig^\rho(s)-ds^T\right)\\&\le\Xi\left(-s^Tk_1s-s^Tk_2sig^\rho(s)+\frac{1}{2}s^Ts+\frac{1}{2}d^2\right)\\&\le-s^T\Xi\left(k_1-\frac{1}{2}\right)s-s^T\Xi k_2sig^\rho(s)+\frac{1}{2}\Xi d^2\\&\le-\frac{\Xi}{2}\left(k_1-\frac{1}{2}\right)V-\frac{\Xi k_2}{2}V^{\frac{1+\rho}{2}}+\frac{1}{2}\Xi d^2\\&\le-\frac{\Xi}{2}\sqrt{k_2\left(k_1-\frac{1}{2}\right)}V^{\frac{3+\rho}{4}}+\frac{1}{2}\Xi d^2\end{aligned} \tag{32}$$

Lemma 1 (Zhen *et al.*, 2011) Define a Lyapunov function on the neighborhood $\Omega(\Omega\in R)$ of the origin. If there exist $l>0,\vartheta>0,0<\mu<1$ that satisfy $\dot{V}(x)+lV^\mu(x)-\vartheta\le0, x\in\Omega$, the system state x can converge to a neighborhood near the origin in a finite time.

According to Lemma1, IADRC is stable and tracking error can converge to the equilibrium point in fixed time .

Section B: convergence analysis of paired coevolution pigeon-inspired optimization

The local convergence condition of optimization algorithm such as PIO and PSO can be described as (Mohammad and Zbigniew, 2016):

$$\forall\xi>0,\lim_{t\to\infty}P\left(\|X_g-X\|<\xi\right)=1 \tag{33}$$

where X_g is the best solution found in search space and X is a particle in optimization process. The convergence of PIO and PSO has been proved by many literatures, so the convergence of PCPIO are analyzed based on the convergence of PIO.

Before the proof, a local minimizer c_i of objective function F is defined over the search space S, which means that in an open

set A_i (c_i is not on the boundary), $\forall x \in A_i, F(c_i) < F(x)$. $R_{\varsigma,i}$ is defined as

$$R_{\varsigma,i} = \{x \in A_i : F(x) < F(c_i) + \varsigma\}$$

where ς is an arbitrarily small positive value. Then the optimal region of F is set as $R_\varsigma = \cup_i R_{\varsigma,i}$. A general form of stochastic algorithms (general stochastic algorithm [GSA]) is defined as follows.

Definition 1: There are three steps in GSA:

- Initialize p_0 from the search space S and set t as 1.
- Generate a random sample x_t from S.
- Generate the candidate solution $p_t = D(p_{t-1}, x_t)$, set $t = t+1$, and go to 2 where $D(a,b)$ is defined by:

$$D(a,b) = \begin{cases} b & F(b) < F(a) - \varsigma_0 \\ a & \text{otherwise} \end{cases}$$

and ς_0 is a positive value that is smaller than or equal to ς (ς is in the definition of $R_{\varsigma,i}$).

Lemma 2 (Mohammad and Zbigniew, 2016): If GSA satisfies the condition:

$$\exists \varepsilon > 0, \exists \eta > 0, \exists \delta \in (0,1], \forall t' > 0, P\left(F(p_{t+t'}) \le F(p_t) - \eta\right) > \delta \text{ or } p_t \in R\varsigma$$

GSA is locally convergent.

Lemma 3 (Mohammad and Zbigniew, 2016): If a GSA meets the following condition:

$$\forall t > 0, \exists z, h > 0, \forall \mu \in R_h(p_t), \forall \varsigma > 0, P(\|x_{t+z} - u\| < \varsigma_0) > 0$$

then the Lemma 2 can be used, which means that if there is an iteration z that x_{t+z} has nonzero probability to be arbitrarilyclose to any point in R_h (p_t) then the condition in Lemma 2 is satisfied.

Proof: Substitute equation (18) into equation (19), and the position of $X_i(t)$ can be expressed as:

$$X_i(t) = X_i(t-1) + V_i(t-1) \cdot e^{-Rt} + rand \cdot \left(X_g - X_i(t-1)\right) \tag{34}$$

Subtract X_g from both sides of equation (34):

$$X_i(t) - X_g = X_i(t-1) - X_g + V_i(t-1) \cdot e^{-Rt} + rand \cdot \left(X_g - X_i(t-1)\right) \tag{35}$$

which can be rewritten as:

$$X_i(t) - X_g = (1 - rand) \cdot \left(X_i(t-1) - X_g\right) + V_i(t-1) \cdot e^{-Rt} \tag{36}$$

Because the search space is a limited, $\forall \varepsilon > 0, \exists t > 0, s.t. \|V_i(t-1) \cdot e^{-Rt}\| < \varepsilon \|X_i(t-1) - X_g\|$. Then take the Euclidean distance from both sides of equation (36),

$$\|X_i(t) - X_g\| < \|1 - rand - \varepsilon\| \cdot \|X_i(t-1) - X_g\| \tag{37}$$

For particle P_i, there are three cases.

Case 1:

If P_i and P_{i+1} (i = 1:2:popsize-1) are not trapped into a local extreme, then P_i and P_{i+1} are going to be updated towards X_g.

Case 2:

If one of P_i and P_{i+1} (i = 1:2:popsize-1) is trapped into a local extreme, taking the case of P_i trapped in a local extremum, then P_{i+1} is going to be updated towards X_g. We can obtain:

$$\begin{cases} P'_{ij}(t) = P_{ij}(t) + \delta_{ij}, t \to \infty \\ P'_{i+1,j}(t) = X_g + \delta_{i+1,j}, t \to \infty \end{cases} \tag{38}$$

$$\begin{cases} P''_i(t) = c \cdot P'_i(t) + (1-c) \cdot P'_{i+1}(t) \\ P''_{i+1}(t) = c \cdot P'_{i+1}(t) + (1-c) \cdot P'_i(t) \end{cases} \tag{39}$$

where δ_{ij} represents a small positive or negative number. Substitute equation (39) into equation (36),

$$\begin{cases} X_{ij}(t+1) - X_g = (1 - rand) \cdot \left(c \cdot \left(P_{ij}(t) + \delta_{ij}\right) + (1-c) \cdot \left(X_{gj} + \delta_{i+1,j}\right) - X_{gj}\right) + V_{ij}(t) \cdot e^{-Rt} \\ X_{i+1,j}(t+1) - X_g = (1 - rand) \cdot \left(c \cdot \left(X_{gj} + \delta_{i+1,j}\right) + (1-c) \cdot \left(P_{ij}(t) + \delta_{ij}\right) - X_{gj}\right) + V_{i+1,j}(t) \cdot e^{-Rt} \end{cases} \tag{40}$$

which can be reestablished as:

$$\begin{cases} X_{ij}(t+1) - X_g = (1 - rand) \cdot c \cdot \left(P_{ij}(t) - X_{gj}\right) + (1 - rand) \cdot \left(c \cdot \left(\delta_{ij} - \delta_{i+1,j}\right) + \delta_{i+1,j}\right) + V_{ij}(t) \cdot e^{-Rt} \\ X_{i+1,j}(t+1) - X_g = (1 - rand) \cdot c \cdot \left(P_{ij}(t) - X_{gj}\right) + (1 - rand) \cdot \left(c \cdot \left(\delta_{i+1,j} - \delta_{ij}\right) + \delta_{ij}\right) + V_{i+1,j}(t) \cdot e^{-Rt} \end{cases} \tag{41}$$

$\forall \varepsilon > 0, \exists t > 0, s.t.$

$$\begin{cases} \|(1-rand)\cdot(c\cdot(\delta_{ij}-\delta_{i+1,j})+\delta_{i+1,j})+V_{ij}(t)\cdot e^{-Rt}\| < \varepsilon\|P_{ij}(t)-X_{gj}\| \\ \|(1-rand)\cdot(c\cdot(\delta_{i+1,j}-\delta_{ij})+\delta_{ij})+V_{i+1,j}(t)\cdot e^{-Rt}\| < \varepsilon\|P_{ij}(t)-X_{gj}\| \end{cases}$$

.

equation (38) can be obtained from equation (41):

$$\begin{cases} \|X_{ij}(t+1)-X_g\| < \|\left(1-rand-\dfrac{\varepsilon}{c}\right)\cdot c\cdot\left(P_{ij}(t)-X_{gj}\right)\| \\ \|X_{i+1,j}(t+1)-X_g\| < \|\left(1-rand-\dfrac{\varepsilon}{c}\right)\cdot c\cdot\left(P_{ij}(t)-X_{gj}\right)\| \end{cases} \tag{42}$$

For particle P_i in P_{best}, there is a region R_i around X_g in which the particle's fitness is smaller than $fitness(P_i)$. When $rand$ is large enough and $X_i(t)$ would jump into R_i.

Case 3:

If P_i and P_{i+1} (i = 1:2:popsize-1) are all trapped into local extreme, equation (38) can be rewritten as:

$$\begin{cases} P'_{ij}(t) = P_{ij}(t)+\delta_{ij}, t\to\infty \\ P'_{i+1,j}(t) = P_{i+1,j}(t)+\delta_{i+1,j}, t\to\infty \end{cases} \tag{43}$$

Equation (40) would be transformed as:

$$\begin{cases} X_{ij}(t+1)-X_g = (1-rand)\cdot\left(c\cdot\left(P_{ij}(t)+\delta_{ij}\right)+(1-c)\cdot\left(P_{i+1,j}(t)+\delta_{i+1,j}\right)-X_{gj}\right)+V_{ij}(t)\cdot e^{-Rt} \\ X_{i+1,j}(t+1)-X_g = (1-rand)\cdot\left(c\cdot\left(P_{i+1,j}(t)+\delta_{i+1,j}\right)+(1-c)\cdot\left(P_{ij}(t)+\delta_{ij}\right)-X_{gj}\right)+V_{i+1,j}(t)\cdot e^{-Rt} \end{cases} \tag{44}$$

which can be reestablished as:

$$\begin{cases} X_{ij}(t+1)-X_g = (1-rand)\cdot\left(c\cdot\left(P_{ij}(t)-P_{i+1,j}(t)\right)+\left(P_{i+1,j}(t)-X_{gj}\right)\right.\ +c\cdot(\delta_{ij}-\delta_{i+1,j})+\delta_{i+1,j})+V_{ij}(t)\cdot e^{-Rt} \\ X_{i+1,j}(t+1)-X_g = (1-rand)\cdot\left(c\cdot\left(P_{i+1,j}(t)-P_{ij}(t)\right)+\left(P_{ij}(t)-X_{gj}\right)\right.\ +c\cdot(\delta_{i+1,j}-\delta_{ij})+\delta_{ij})+V_{i+1,j}(t)\cdot e^{-Rt} \end{cases} \tag{45}$$

Obviously, it can be deduced by equation (45) as follows:

$$\begin{cases} \|X_{ij}(t+1)-X_g\| < \|(1-rand)\cdot\left(c\cdot\left(P_{ij}(t)-P_{i+1,j}(t)\right)+(1-\varepsilon)\cdot\left(P_{i+1,j}(t)-X_{gj}\right)\right)\| \\ \|X_{i+1,j}(t+1)-X_g\| < \|(1-rand)\cdot\left(c\cdot\left(P_{i+1,j}(t)-P_{ij}(t)\right)+(1-\varepsilon)\cdot\left(P_{ij}(t)-X_{gj}\right)\right)\| \end{cases} \tag{46}$$

Similar to Case 2, When $rand$ is large enough and $X_i(t)$ would jump into R_i. So, the particles of P_{best} can jump out local extreme when t approaches infinite. Then all particles will move toward X_g as same as PIO. According to the convergence of Lemma 2 and Lemma 3, we can know that PCPIO is also convergent.

Table 1 Parameters of the algorithms

Algorithm	Variable	Description	Value
PIO/PCPIO	N_{c1max}	Maximum iteration of operator 1	90
	N_{c2max}	Maximum iteration of operator 2	10
	R	Map and compass operator	0.02
GA	P_c	Crossover probability	0.9
	P_m	Mutation probability	0.1
PSO	w	Inertial weight	0.8
	c_1	Learning factor - cognitive constant	1.3
	c_2	Learning factor - social constant	1.5

Table 2 Statistics of simulation results on roll angle

Methods	GA	PIO	PSO	PCPIO
Mean	1.97e-3	2.20e-3	1.40e-3	**1.33e-3**
Std	1.70e-4	8.96e-4	1.33e-4	**9.82e-5**
Best	1.68e-3	1.30e-3	1.22e-3	**1.20e-3**
Worst	2.23e-3	3.28e-3	1.60e-3	**1.50e-3**

Table 3 Statistics of simulation results on pitch angle

Methods	GA	PIO	PSO	PCPIO
Mean	1.78e-3	1.63e-3	1.32e-3	**1.28e-3**
Std	1.37e-4	2.51e-4	9.47e-5	**9.29e-5**
Best	1.68e-3	1.27e-3	1.26e-3	**1.21e-3**
Worst	1.98e-3	1.81e-3	1.46e-3	**1.41e-3**

Table 4 Statistics of simulation results on yaw angle

Methods	GA	PIO	PSO	PCPIO
Mean	1.97e-3	1.33e-3	1.22e-3	**1.13e-3**
Std	2.89e-4	2.29e-4	1.69e-4	**4.79e-5**
Best	1.55e-3	1.14e-3	1.09e-3	**1.07e-3**
Worst	2.35e-3	1.74e-3	1.53e-3	**1.20e-3**

Simulation results and analysis

Series of experiments are conducted for our analysis. All experiments are performed using MATLAB R2018b on a PC with 6 Cores 1.1 GHz CPU and 16 G RAM.

A. Parameters tuning using optimization algorithms

To verify the competence of PCPIO, comparative experiments are set via GA、PIO and PSO with a maximum iteration of 50 and population size of 20. The parameters of the algorithms are listed in Table 1.

To evaluate the effectiveness of selected algorithms fairly, all algorithms use the same initialization results, and 10 separate experiments are conducted on roll angle, pitch angle and yaw angle respectively. The reference of each attitude angle is set to a step signal of 5°, and the mean, standard deviation (std), minimum and maximum for 10 random runs of different methods are showed in Table 2, Table 3 and Table 4.

As shown in Table 2,Table 3 and Table 4, the mean, std, best and worst value of PCPIO are almost always smaller than those of other methods. It can be seen from the data statistics that the optimization performance is sorted as PCPIO, PSO, PIO and GA, respectively. Compared with original PIO, average proportion of PCPIO is 60.5%, 78.5% and 85.0% in roll, pitch and yaw angle, respectively and std proportion is 11.0%, 36.9% and 20.9%, which means that overall optimization effect of PCPIO is better and more stable than that of PIO. Individually, PCPIO has better performance in both the best and the worst outcomes. Similarly, the

Figure 4 Evolutionary Results of roll angle

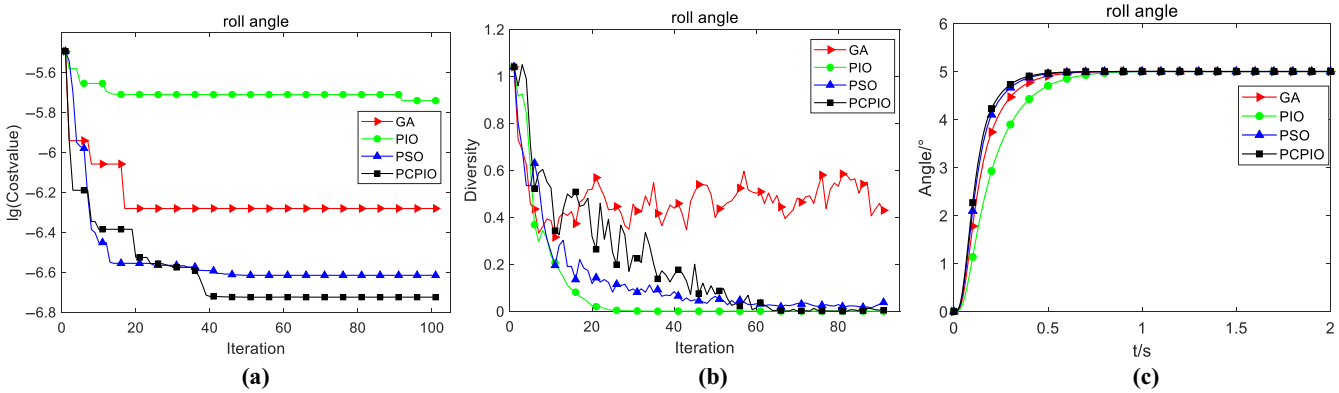

Notes: (a) Evolutionary curve of cost function; (b) Evolutionary curve of diversity; (c) Output re-sponse

Figure 5 Evolutionary Results of pitch angle

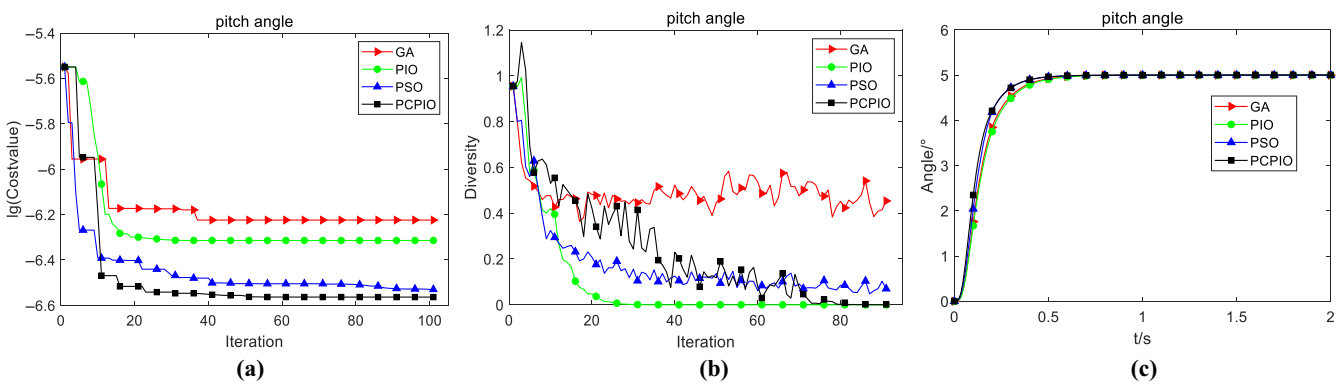

Notes: (a) Evolutionary curve of cost function; (b) Evolutionary curve of diversity; (c) Output re-sponse

Figure 6 Evolutionary Results of yaw angle

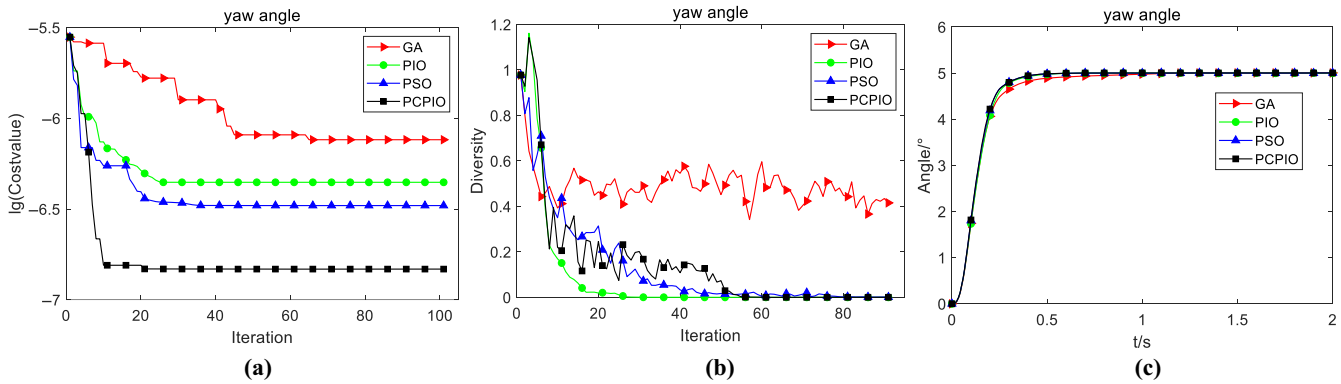

Notes: Evolutionary curve of cost function; (b) Evolutionary curve of diversity; (c) Output response

same result can be obtained in the comparison of PCPIO, PSO and GA, which indicates that PCPIO has stronger search ability and more stable performance than other algorithms.

Figures 4, 5 and 6 are evolutionary results of three angle control channels by different methods, respectively. As the cost value after optimization is very small, it is difficult to directly observe the advantages and disadvantages of different algorithms with original data. Therefore, logarithmic function is applied to process the cost value. Final cost value of PCPIO is minimum in Figures 4(a), 5(a) and 6(a). As shown in Figure 4(b), 5(b) and 6(b), GA has a low optimization speed with a high diversity, while PIO has a faster optimization speed with a low diversity. Combining the advantages of PIO and GA, PCPIO has a high diversity while maintaining a good optimization speed, and it can still jump out of the local extremum after being trapped in local convergence. And the downward trend of diversity of PCPIO is clear, which also reflect the convergence of PCPIO from the side. As shown in Figure 4(c), 5(c) and 6(c), the response obtained by other methods has risen slower and later to reach the target angle than signal optimized by PCPIO.

Figure 7 Pitch angle comparison of different controllers in scenario 1

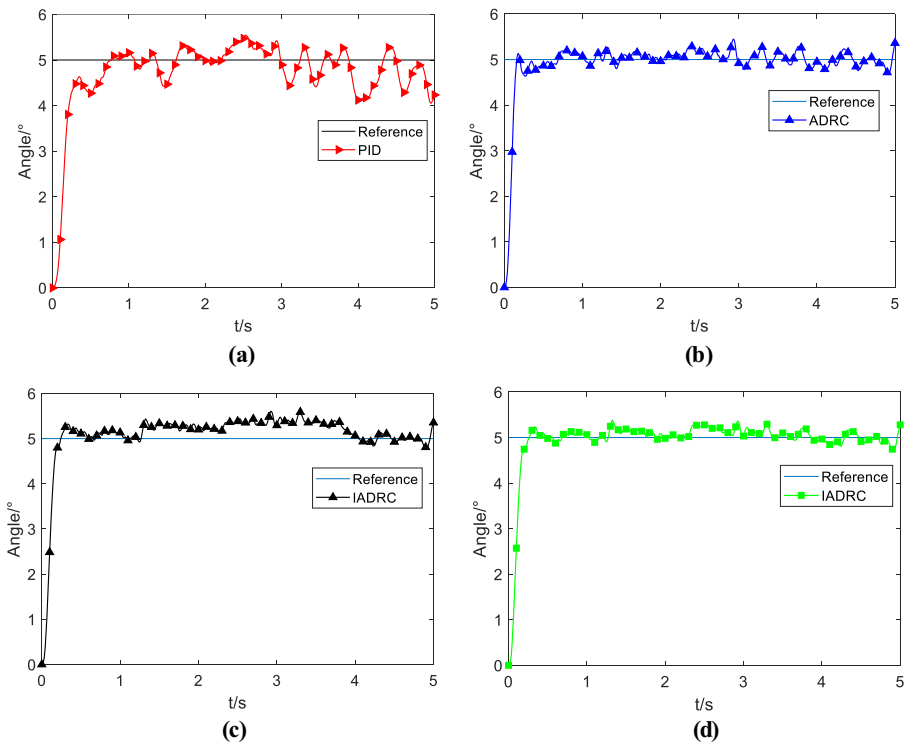

Notes: (a) PID adjusted by Ziegler-Nichols method; (b) ADRC optimized by PCPIO; (c) IADRC ad-justed by Ziegler-Nichols method; (d) IADRC optimized by PCPIO

Figure 8 Pitch angle comparison of different controllers in scenario 2

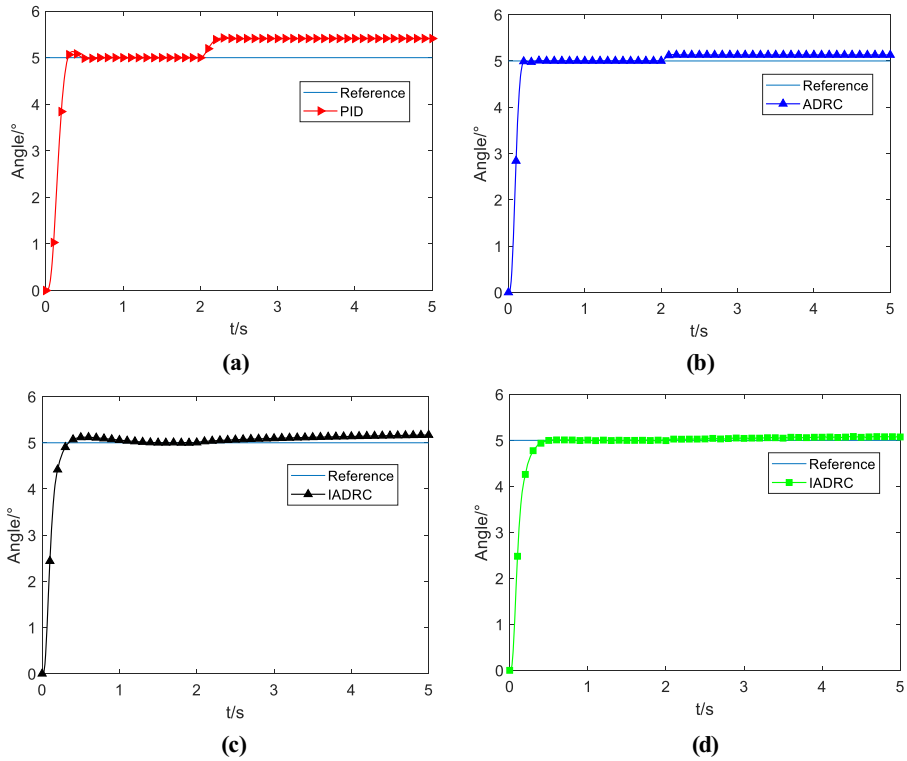

Notes: (a) PID adjusted by Ziegler-Nichols method; (b) ADRC optimized by PCPIO; (c) IADRC ad-justed by Ziegler–Nichols method; (d) IADRC optimized by PCPIO

B. Controllers comparison in different scenarios

To evaluate the anti-disturbance ability of IADRC, a number of comparative experiments are carried out in different scenarios. A total of four controllers are used In comparison, respectively PID adjusted according to Ziegler–Nichols method (Ziegler and Nichols, 1942), ADCRC optimized by PCPIO, IADRC adjusted by Ziegler–-Nichols method and IADRC optimized by PCPIO.

In first scenario, quadrotor has the mission that fly straight from one point to another point. After climbing to a height of 10 meters and hovering, the quadrotor moves along the x-axis to target point with a constant pitch angle of 5°, and a white noise with power of 0.1 is set to continuous disturbance of three angle channels. The simulation results of pitch angle are shown in Figure 7.

It can be seen that the ranking of anti-interference effect is IADRC optimized by PCPIO, ADRC optimized by PCPIO, IADRC adjusted by Ziegler–Nichols method and PID adjusted by Ziegler-Nichols method, and the maximum errors of the four methods after stabilization are 0.914°, 0.602°, 0.447°, 0.375°, respectively. The control effect of IADRC has been greatly improved with PCPIO optimization, and actual pitch angle in Figure 7(d) is closer to the reference value than Figure 7(c). Compared with ADRC, although both pitch angle in Figure 7(d) and (b) has been optimized by PCPIO, the fluctuation of IADRC is smaller and the angle curve is smoother.

In second scenario, the quadrotor is also moving to the target with a constant pitch angle of 5°, while a suddenly disturbance of 0.1 rad/s is added to three angle channels, and the results are shown in Figure 8.

Observing the control effect of the four controllers after the sudden addition of interference, the stabilization error of PID is the largest and that of the optimized IADRC is the smallest. The stabilization error of the unoptimized IADRC increases gradually after adding interference, and is close to the stabilization error of ADRC, while the stabilization error of the optimized IADRC almost remains unchanged at the reference value.

In third scenario, after climbing to a certain altitude, the quadrotor begins to rotate around the Z-axis at a certain angular velocity to carry out the reconnaissance mission. The random disturbance with power of 1 is added during this process.

As shown in Figure 9(a), PID has slow tracking speed, long delay time and strong fluctuation under interference. The tracking speed of ADRC in Figure 9(b) is faster than that of PID, and the anti-interference ability is much stronger. The tracking speed of unoptimized IADRC in Figure 9(c) is slightly faster than ADRC, but it is slower than optimized IADRC in Figure 9(d).

Through the simulation of the above three scenarios, it can be seen that IADRC has stronger anti-disturbance ability and faster tracking speed than ADRC, which is meaningful for the improvement of ADRC.

Figure 9 Yaw angle comparison of different controllers in Scenario 3

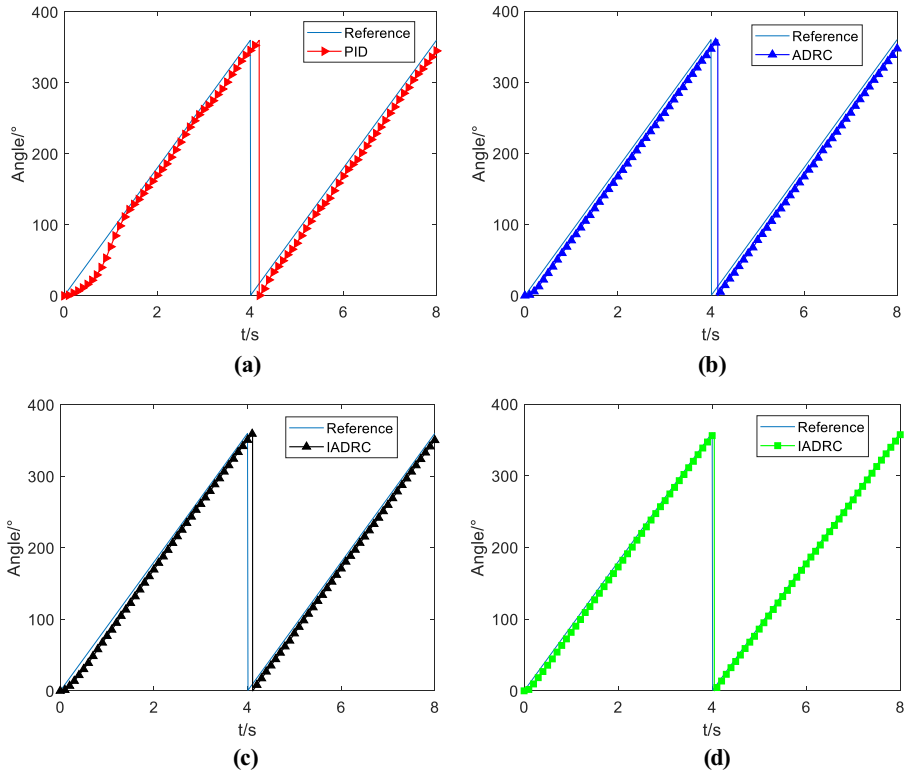

Notes: (a) PID adjusted by Ziegler-Nichols method; (b) ADRC optimized by PCPIO; (c) IADRC ad-justed by Ziegler–Nichols method; (d) IADRC optimized by PCPIO

Conclusions

In general, a quadrotor is difficult to maintain precise attitude control in the case of outdoor flight with disturbance. This paper deigned IADRC attitude controllers to improve anti-disturbance ability and PCPIO algorithm is applied to optimize control parameters to replace trial and error tuning method. NFTSM control law and TOTD is designed for proposed IADRC, which shows higher control accuracy and better robustness than ADRC. And evolutionary mechanism introduced in PCPIO has overcome the problem of rapid decline of population diversity and increase the individual optimality of all pigeons with a probability factor opposite to population diversity. A series of simulation experiments are carried out to verify the feasibility and efficiency of the proposed IADRC and PCPIO, which shows the improvement of IADRC and PCPIO are significant.

References

Alazzam, A., Sharieh, A. and Sabri, K.E. (2020), "A feature selection algorithm for intrusion detection system based on pigeon inspired optimizer", *Expert Systems with Applications*, Vol. 148.

Bartoszewicz, A. and Nowacka-Leverton, A. (2010), "ITAE optimal sliding modes for third-order systems with input signal and state constraints", *IEEE Transactions on Automatic Control*, Vol. 55 No. 8, pp. 1928-1932.

Deng, Y. and Duan, H. (2016), "Control parameter design for automatic carrier landing system via pigeon-inspired optimization", *Nonlinear Dynamics*, Vol. 85 No. 1, pp. 97-106.

Duan, H., Huo, M. and Yang, Z. (2019), "Predator-prey pigeon-inspired optimization for UAV ALS longitudinal parameters tuning", *IEEE Transactions on Aerospace and Electronic Systems*, Vol. 55 No. 5, pp. 2347-2358.

Duan, H. and Qiao, P. (2014), "Pigeon-inspired optimization: a new swarm intelligence optimizer for air robot path planning", *International Journal of Intelligent Computing and Cybernetics*, Vol. 7 No. 1, pp. 24-37.

Duan, H. and Wang, X. (2016), "Echo state networks with orthogonal pigeon-unspired optimization for image restoration", *IEEE Transactions on Neural Networks and Learning Systems*, Vol. 27 No. 11, pp. 2413-2425.

Emam, M. and Fakharian, A. (2016), "Attitude tracking of quadrotor UAV via mixed H2/H∞ controller: an LMI based approach", *24th Mediterranean Conference on Control and Automation (MED)*, pp. 390-395.

Guo, B. and Zhao, Z. (2011), "On the convergence of an extended state observer for nonlinear systems with uncertainty", *Systems & Control Letters*, Vol. 60 No. 6, pp. 420-430.

Hai, X., Wang, Z. and Feng, Q. (2019), "Mobile robot ADRC with an automatic parameter tuning mechanism via modified pigeon-inspired optimization", *IEEE/ASME Transactions on Mechatronics*, Vol. 24 No. 6, pp. 2616-2626.

Han, J. (2009), "From PID to active disturbance rejection control", *IEEE Transactions on Industrial Electronics*, Vol. 56 No. 3, pp. 900-906.

Kennedy, J. and Eberhart, R. (1995), "Particle swarm optimization", *Proceedings of ICNN'95 - International Conference on Neural Networks*, Vol. 4, pp. 1942-1948.

Labbadi, M. and Cherkaoui, M. (2019), "Robust adaptive backstepping fast terminal sliding mode controller for uncertain quadrotor UAV", *Aerospace Science and Technology*, Vol. 93.

Ma, X., Guo, Y. and Chen, L. (2018), "Active disturbance rejection control for electric power steering system with assist motor variable mode", *Journal of the Franklin Institute*, Vol. 355 No. 3, pp. 1139-1155.

Mohammad, R.B. and Zbigniew, M. (2016), "Analysis of stability, local convergence, and transformation sensitivity of a variant of the particle swarm optimization algorithm", *IEEE Transactions on Evolutionary Computation*, Vol. 20 No. 3, pp. 370-385.

Muhammad, T., Li, A. and Rooh, uA. (2019), "Disturbances rejection based on sliding mode control", *Aircraft Engineering and Aerospace Technology*, Vol. 91 No. 4, pp. 680-699.

Oliva-Palomo, F., Munoz-Vazquez, A.J. and Sanchez-Orta, A. (2019), "A fractional nonlinear PI-structure control for robust attitude tracking of quadrotors", *IEEE Transactions on Aerospace and Electronic Systems*, Vol. 55 No. 6, pp. 2911-2920.

Quan, Q. (2007), "*Introduction to Multicopter Design and Control*", Springer, Singapore.

Ramirez-Rodriguez, H., Parra-Vega, V., Sanchez-Orta, A. and Garcia-Salazar, O. (2014), "Robust backstepping control based on integral sliding modes for tracking of quadrotors", *Journal of Intelligent & Robotic Systems*, Vol. 73 Nos 1/4, pp. 51-66.

Raza, S.A., Sutherland, M., Etele, J. and Fusina, G. (2017), "Experimental validation of quadrotor simulation tool for flight within building wakes", *Aerospace Science and Technology*, Vol. 67, pp. 169-180.

Rooh, uA., Irum, I. and Li, A.J. (2019), "Finite time position and heading tracking control of coaxial octorotor based on extended inverse multi-quadratic radial basis function network and external disturbance observer", *Journal of the Franklin Institute*, Vol. 356, pp. 4240-4269.

Roohul, A., Li, A. and Shahaboddin, S. (2016), "A review of quadrotor UAV: control methodologies and performance evaluation", *International Journal of Automation and Control*, Vol. 10 No. 2, pp. 87-103.

Shao, X., Liu, J. and Wang, H. (2018), "Robust back-stepping output feedback trajectory tracking for quadrotors via extended state observer and sigmoid tracking differentiator", *Mechanical Systems and Signal Processing*, Vol. 104, pp. 631-647.

Srinivas, M. and Patnaik, L.M. (1994), "Adaptive probabilities of crossover and mutation in genetic algorithms", *IEEE Transactions on Systems, Man, and Cybernetics*, Vol. 24 No. 4, pp. 656-667.

Tian, B., Zuo, Z. and Zong, Q. (2019), "Adaptive finite-time attitude tracking of quadrotors with experiments and comparisons", *IEEE Transactions on Industrial Electronics*, Vol. 66 No. 12, pp. 9428-9438.

Wang, B., Shen, Y. and Zhang, Y. (2020), "Active fault-tolerant control for a quadrotor helicopter against actuator faults and model uncertainties", *Aerospace Science and Technology*, Vol. 99.

Wu, Y. and Li, G. (2018), "Adaptive disturbance compensation finite control set optimal control for PMSM systems based on sliding mode ex-tended state observer", *Mechanical Systems and Signal Processing*, Vol. 98, pp. 402-414.

Yang, Q., Chen, W. and Deng, J. (2018a), "A level-based learning swarm optimizer for large-scale optimization", *IEEE Transactions on Evolutionary Computation*, Vol. 22 No. 4, pp. 578-594.

Yang, H., Cheng, L., Xia, Y. and Yuan, Y. (2018b), "Active disturbance rejection attitude control for a dual closed-loop quadrotor under gust wind", *IEEE Transactions on Control Systems Technology*, Vol. 26 No. 4, pp. 1400-1405.

Yang, L. and Lu, Z. (2006), "Proof of a third-order tracking differentiator's convergence and simulation of its dynamic characteristics", *Journal of Yanshan University*, No. 1, pp. 44-47.

Zhang, B. and Duan, H. (2017), "Three-dimensional path planning for uninhabited combat aerial vehicle based on predator-prey pigeon-inspired optimization in dynamic environment", *IEEE/ACM Transactions on Computational Biology and Bioinformatics*, Vol. 14 No. 1, pp. 97-107.

Zhao, S., An, H., Zhang, D. and Shen, L. (2016), ""A new feedback linearization LQR control for attitude of quadrotor", *13th international conference on control*", *Automation, Robotics & Vision*, pp. 1593-1597.

Zhao, L., Dai, L., Xia, Y. and Li, P. (2019), "Attitude control for quadrotors subjected to wind disturbances via active disturbance rejection control and integral sliding mode control", *Mechanical Systems and Signal Processing*, Vol. 129, pp. 531-545.

Zhao, Z. and Guo, B. (2015), "Extended state observer for uncertain lower triangular nonlinear systems", *Systems & Control Letters*, Vol. 85, pp. 100-108.

Zhen, Z., Xia, Y. and Fu, M. (2011), "Attitude stabilization of rigid spacecraft with finite-time convergence", *International Journal of Robust and Nonlinear Control*, Vol. 21 No. 6, pp. 686-702.

Ziegler, J.G. and Nichols, N.B. (1942), "Optimum settings for automatic controllers", *Transactions of the ASME*, Vol. 64, pp. 759-768.

Corresponding author

Haibin Duan can be contacted at: hbduan@buaa.edu.cn